DOI:10.25092/baunfbed. 1659472 *J. BAUN Inst. Sci. Technol., 27(2), 626-638, (2025)*

Effect of line-width parameter on the tensile strength, surface profile and printing time of 3D printed PLA parts

Ahmet Çağrı KILINÇ*

Osmaniye Korkut Ata University Faculty of Engineering and Natural Sciences, Department of Mechanical Engineering, Fakıuşağı Campus, Osmaniye.

Geliş Tarihi (Received Date): 17.03.2025
Kabul Tarihi (Accepted Date): 22.04.2025

Abstract

This study investigates the effect of line-width values on the properties of 3D (three dimensional) printed PLA (polylactic acid) parts. 3D printing of parts was carried out by using low-cost cartesian type FFF (fused filament fabrication) desktop 3D printer. Brass nozzle with a diameter of 0.6 mm was used to print PLA parts. Parts having line-width values of 0.6 mm to 1.2 mm were printed and the effect of line-width values on the mechanical properties and printing time was investigated. Mechanical properties of 3D printed parts were determined by using tensile testing device (Zwick/Roell, Z250). Microstructures of 3D printed samples were investigated by using optical microscope (Leica, DM 2500). Printing time for each part was recorded during 3D printing process. Surface profiles of parts were investigated by using surface roughness tester (Mitutoyo SJ-210). Microstructural investigations showed that the voids were formed between adjacent deposited lines and the void content decreased from 5.89% to 5.13% with increasing line-width value up to 1.0 mm. Surface roughness parameter of Ra increased from 5.11±0.21 µm to 9.29±1.12 µm with increasing line-width. Tensile strength of 3D printed specimens showed a slight decrease with increasing line-width due to the presence of voids between adjacent u-turn sections. The tensile strength values were determined as 58.52±1.93 MPa and 46.54±1.18 MPa for specimens printed with line-width values of 0.6 mm and 1.2 mm respectively. SEM images of tensile fracture surface demonstrated that the main failure mechanism of the printed specimens was the rupture of deposited lines instead of fracture of inter-line bonding.

Keywords: *3D printing, mechanical properties, characterization.*

* Ahmet Çağrı KILINÇ, ahmetcagrikilinc@osmaniye.edu.tr, https://orcid.org/0000-0003-1705-5676

Hat-genişliği parametresinin 3B yazdırılmış PLA parçaların çekme mukavemeti, yüzey profili ve yazdırma süresi üzerindeki etkisi

Öz

Bu çalışma, hat-genişliği değerlerinin 3B (üç boyutlu) yazdırılmış PLA (polilaktik asit) parçalarının özellikleri üzerindeki etkisini incelemektedir. Parçaların 3B yazdırma, düşük maliyetli kartezyen tip FFF (eriyik filament üretimi) masaüstü 3B yazıcı kullanılarak gerçekleştirildi. PLA parçaları yazdırmak için 0,6 mm çapında pirinç nozul kullanıldı. 0,6 mm ile 1,2 mm arasında hat genişliği değerlerine sahip parçalar basıldı ve hat genişliği değerlerinin mekanik özellikler ve yazdırma süresi üzerindeki etkisi incelendi. 3B yazdırılmış parçaların mekanik özellikleri, çekme test cihazı (Zwick/Roell, Z250) kullanılarak belirlendi. 3B yazdırılmış numunelerin mikro yapıları optik mikroskop (Leica, DM 2500) kullanılarak incelendi. 3D yazdırma işlemi sırasında her parça için yazdırma süresi kaydedildi. Parçaların yüzey profilleri yüzey pürüzlülük test cihazı (Mitutoyo SJ-210) kullanılarak incelendi. Mikroyapısal incelemeler, boşlukların bitişik depozitlenmiş hatlar arasında oluştuğunu ve boşluk içeriğinin 1,0 mm'ye kadar artan hat genişliği değeriyle %5,89'dan %5,13'e düştüğünü gösterdi. Yüzey pürüzlülük parametresi Ra, artan hat genişliğiyle 5.11±0.21 µm'den 9.29±1.12 µm'ye yükseldi. 3B yazdırılmış numunelerin çekme mukavemeti, bitişik u-dönüşü bölümleri arasındaki boşlukların varlığı nedeniyle artan hat genişliğiyle azalma gösterdi. Çekme mukavemeti değerleri, 0,6 mm ve 1,2 mm hat genişliği değerleriyle yazdırılmış numuneler için sırasıyla 58.52±1.93 MPa ve 46.54±1.18 MPa olarak belirlendi. Çekme kırılma yüzeyinin SEM görüntüleri, yazdırılmış numunelerin ana hasar mekanizmasının, hatlar arası bağların kırılması yerine depozitlenmiş hatların kopması olduğunu gösterdi.

Anahtar kelimeler: *3B yazdırma, mekanik özellikler, karakterizasyon.*

1. Introduction

Additive manufacturing (AM) offers advantages such as low-cost production of customized products and design flexibility in complex geometries [1]. AM is defined as the layered manufacturing of parts based on digital design files. This technology covers the stacking of layers on top of each other to form the part [2] [3]. AM technology includes many production techniques such as binder jetting, selective laser sintering and melting (SLS and SLM), digital light processing (DLP) and fused filament fabrication (FFF). Among these techniques, the FFF method is one of the most widely used because of low cost and being easily accessible [4]. In the FFF method, polymeric filaments with a customized diameter of 1.75 mm are generally used [5]. The polymeric filament is transferred to the temperature-controlled heating area by a stepper motor. The polymeric material that transferred to the heating area melts and the melted polymer is deposited as an individual line extruded from the nozzle mouth to the build table. Deposited lines with a stable width are obtained by transfer of the filament at a certain speed by the stepper motor. Layers are obtained by deposition of individual lines adjacently in a controlled manner, and the final product is produced by depositing these layers on top of each other in a controlled manner [6].

Although many polymeric materials such as polypropylene (PP), polyethylene terephthalate (PET), thermoplastic elastomer (TPU), acrylonitrile butadiene styrene (ABS), are used as filaments in 3D printing, PLA is one of the most popular thermoplastic materials used in FFF method because of its biodegradable, biocompatible characteristics and relatively high strength properties [7].

Properties of 3D printed PLA parts strongly depend on the printing parameters which are determined during the slicing process such as printing temperature, printing speed, infill ratio, infill type, layer thickness and build orientation and nozzle size [8]. The literature review showed that the effect of these parameters on the properties of 3D printed parts was widely studied in detail. Chacón et al. (2017) investigated the effect of build orientation, layer thickness and feed rate/flow rate on the mechanical properties of 3D printed PLA parts [8]. Kuznetsov et al. (2018) investigated the effect of nozzle diameter and layer thickness on the bonding strength between adjacent layers as a function of geometrical parameters of the FFF process [9]. Molina et al. (2025) focused on the effect of nozzle temperature, layer thickness and raster angle on the mechanical properties of 3D printed specimens by using ABS and PLA filaments [10]. Although literature studies mainly focused on the effects of printing parameters on the mechanical properties of the parts, some studies examined the effects on printing time and surface properties in addition to mechanical properties. For example, Bhosale et al. (2022) investigated the effects of printing speed, layer thickness and infill percentage on the mechanical properties of the parts as well as the surface profile and printing time [11]. Although different printing parameters were examined in the literature as described above, the effect of line-width was ignored and there are limited experimental studies that examine the effect of line-width on mechanical properties, surface roughness, and production time [12-14].

Although the use of nozzles with different diameters is an option for the getting of wider deposited lines, the alteration of the line-width while using same nozzle is another simple way. Therefore, this study focused on the effect of line-width change on the properties of 3D printed parts while using same nozzle (0.6 mm). Effect of line-width change on the void content, surface profile and printing time as well as the mechanical properties such as tensile strength and hardness were investigated within the scope of the study.

2. Material and method

2.1. Material

Natural PLA filament with a filament diameter of 1.75 mm was used for 3D printing of parts. The filament was supplied by ESUN (Shenzhen, China). The filament contained no additives, pigments or coloring agents. Properties of the filament supplied by the manufacturer were given in Table 1.

Table 1. Properties of PLA filament

Properties	**Unit**
Melt Flow Index (MFI)	5 (190°C/2.16kg)
Density	1.23 g/cm^3
Heat distortion Temperature	53 °C

2.2. 3D Printing Process

3D printing of PLA parts was carried out by using custom made cartesian type desktop 3D printer whose printhead moves in the X and Z axis while the build plate moves in the Y axis. The 3D printer has a printing volume of 150 mm *150 mm *150 mm (x*y*z). The image of 3D printer and 3D printing process were shown in Figure 1. a and b respectively.

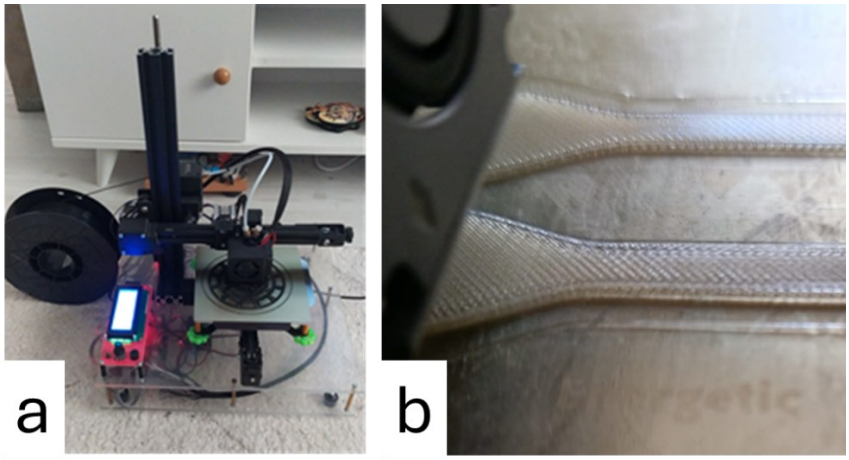

Figure 1. a) 3D printer and b) printing process

Slicing program was used to generate geometric code (gcode) files that contain instructions for controlling computerized machine tools and 3D printers such as tool path and printing settings in the form of G and M codes and comment lines [15]. Samples were produced by stacking deposited layers one top of another and the layers were formed by the sequential arrangement of individual deposited lines from the nozzle according to gcode file produced by slicing process of digital designs. The printing speed and printing temperature were fixed for all samples and kept in the manufacturer recommended limit values. All samples were printed at a nozzle temperature of 210 °C and 40 mm/s of printing speed. The printing speed refers to the movement speed of nozzle. The detailed 3D printing parameters were given in Table 2.

Table 2. 3D printing parameters

Parameter	**Unit**
Printing temperature	210 °C
Printing speed	40 mm/s
Bed temperature	60 °C
Infill type	Rectilinear
Infill density	100%
Infill angle	45°/-45°
Layer height	0.2 mm
Nozzle diameter	0.6 mm
Wall count	1
Line-width	0.6, 0.8, 1 and 1.2 mm

2.3. Characterization

Thermal behavior of PLA filament was investigated by thermogravimetric analysis (TGA). The TGA test was conducted by using thermal analyzer (Hitachi Exstar 7300). Samples were heated from room temperature to 600 °C with a heating ramp of 10 °C/min under nitrogen atmosphere. Tensile properties of samples were determined by using tensile testing. Tensile testing samples were printed according to ASTM D638 and tests were conducted by using universal testing device (Zwick/Roell, Z250) with a cross-head speed of 10 mm/min. Schematic representation and image of tensile test specimens are shown in Figure 2. Three replications were performed for tensile testing. Tensile fracture surface of samples was investigated by using scanning electron microscope (SEM) (JEOL/JCM-5000). Fracture surface of samples was sputter coated with Au-Pd prior to SEM observations to make surface of polymer conductive and prevent electron charging problems during examinations.

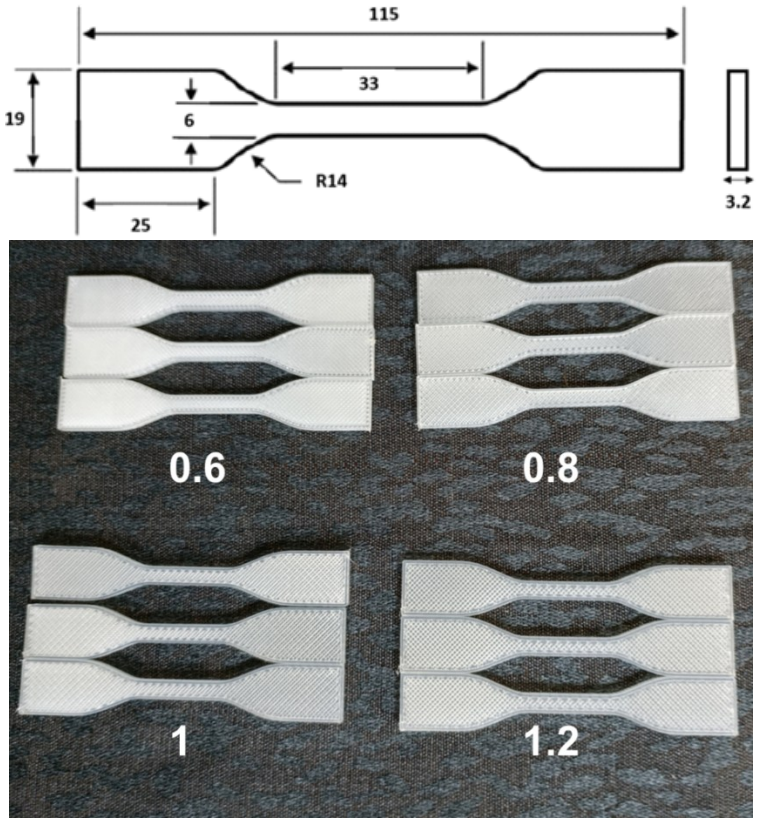

Figure 2. Schematic representation and image of tensile test specimens.

Porosity values of printed samples were determined by optical microscope (Leica, DM 2500). Samples were ground by using 80 to 800 grit sandpapers and polished by using polishing paste containing particles with a particle size of 6 µm. ImageJ which is an open access image analysis program was used for determination of porosity content. The amount of porosity measured from the investigation cross-sectional optical microscope images. The hardness of samples was measured by using Shore-D hardness tester. Specimens with dimensions of 40 mm *15 mm *5 mm (x*y*z) were printed for hardness and surface roughness measurements. Five replications were performed for hardness testing. The printing time of the process for each sample was recorded. Surface roughness of samples printed with various line-width values were measured by using surface roughness tester (Mitutoyo SJ-210). The process of surface roughness and hardness

measurements are shown in Figure 3 a and b respectively. Three different sections of specimens were measured for determination of surface roughness.

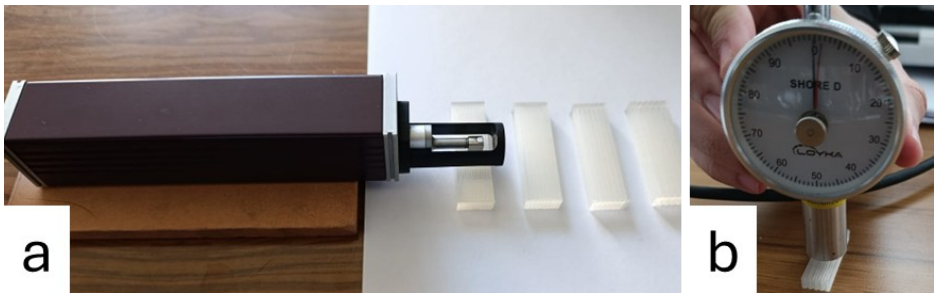

Figure 3. Images of a) surface roughness, and b) Shore-D hardness measurements.

3. Results and discussion

Thermogravimetric analysis (TGA), differential thermal analysis (DTA) and derivative thermal gravimetric (DTG) curves of PLA are shown in Figure 4. TGA curve of PLA demonstrated that the mass loss of polymer started at the temperature of 298 °C and continued up to the temperature of 397 °C. DTA curve of PLA demonstrated that endothermic and exothermic reactions occurred during heating of the polymer. The first peak located at 67 °C refers to the glass transition. Similar temperature of glass transition for PLA was reported by Chen et al. (2020) [16]. The second peak referring to a crystallization exotherm located at 107 °C. This crystallization is called cold crystallization. The small exothermic peak located at 168 °C corresponds to melt crystallization [17]. The endothermic peak located at 182 °C occurred due to the melting of polymer [18]. The sharp endothermic peak located at 372 °C refers to the decomposition of polymeric chains [19]. DTG curve exhibited single step sharp peak located at 373 °C which corresponds to the temperature of the maximum mass loss rate [20].

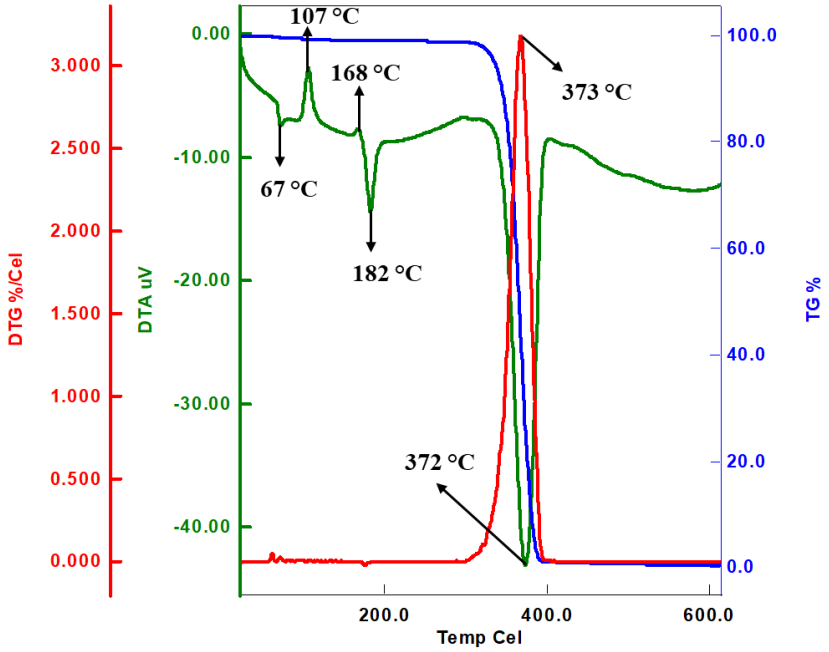

Figure 4. TGA, DTA and DTG curves of PLA filament.

Optical microscope images prepared for porosity measurement were shown in Figure 5 a-d. Porosity values of specimens 3D printed by using line-width values of 0.6 mm, 0.8 mm, 1 mm and 1.2 mm were determined according to areal ratio of voids by using ImageJ free access program. Porosity values were determined as 5.89%, 5.60%, 5.13% and 7.42% for specimens 3D printed with line-width values of 0.6 mm, 0.8 mm, 1 mm and 1.2 mm respectively. The measurements of porosity amount demonstrated that increasing line width results in decreased porosity except for the specimen printed with 1.2 mm line-width. As seen in Figure 5, the layers were deposited uniformly on each other and the gaps were formed on a linear direction, which indicates that there was no layer-shifting problem during printing. It is clearly seen that the void geometry did not change with increasing line width (except 1.2 mm), but the distance between the voids increased as expected. By increasing the line width to 1.2 mm, a change in the gap geometry was observed. It was observed that some lines were not deposited adjacent to each other and accordingly the void size increased in the Z axis, indicating poor bead to bead adhesion [21].

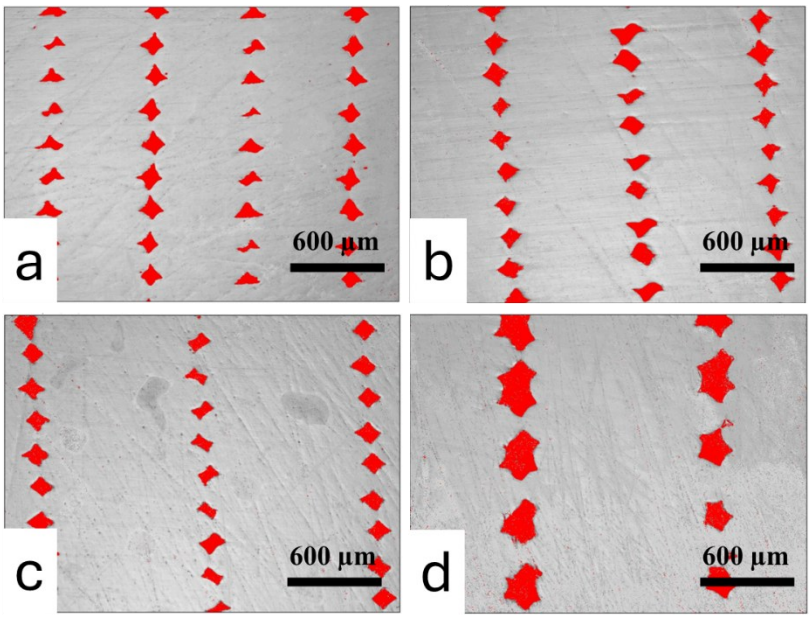

Figure 5. Optical cross-sectional images of 3D printed specimens with a line-width value of a) 0.6 mm, b) 0.8 mm, c) 1 mm and d) 1.2 mm.

The shape of the extruded line is actually cylinder and therefore the cross-sectional shape resembles a circle. An increase in the ratio of nozzle diameter to layer thickness causes the circular cross-section shape to become compressed ellipse or elongated rectangle [9]. The void was formed as a result of adjacent deposition of these lines. The cross-sectional geometry of void between these adjacently deposited lines resembled rhombus-like shape and called as inter-bead void. The mechanism of inter-bead void formation is shown in Figure 6.

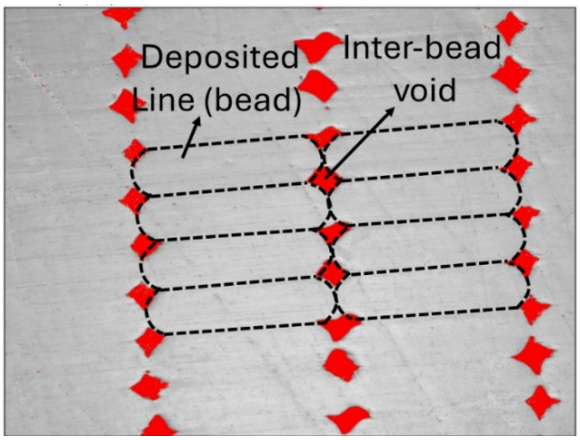

Figure 6. The mechanism of inter-bead void formation

Surface profiles of 3D printed specimens with line-width values of 0.6 mm to 1.2 mm were shown in Figure 7 a to d respectively. As it is seen from the figure that surface profile curves depicts clear 3D printing profile. Individual lines are clearly noticeable and each pit which corresponds to contact regions of adjacent deposited lines moves apart from each other with increasing line-width from 0.6 mm to 1.2 mm. Surface roughness parameters of Ra, Rq and Rz are given in Table 3. It was observed that the surface roughness increased from 5.11±0.21 µm, 6.67±0.48 µm and 36.18±4.31 µm to 9.29±1.12 µm, 13.95±1.58 µm and 66.58±9.41 µm for the parameters of Ra, Rq and Rz respectively with an increasing line-width value from 0.6 mm to 1.2 mm.

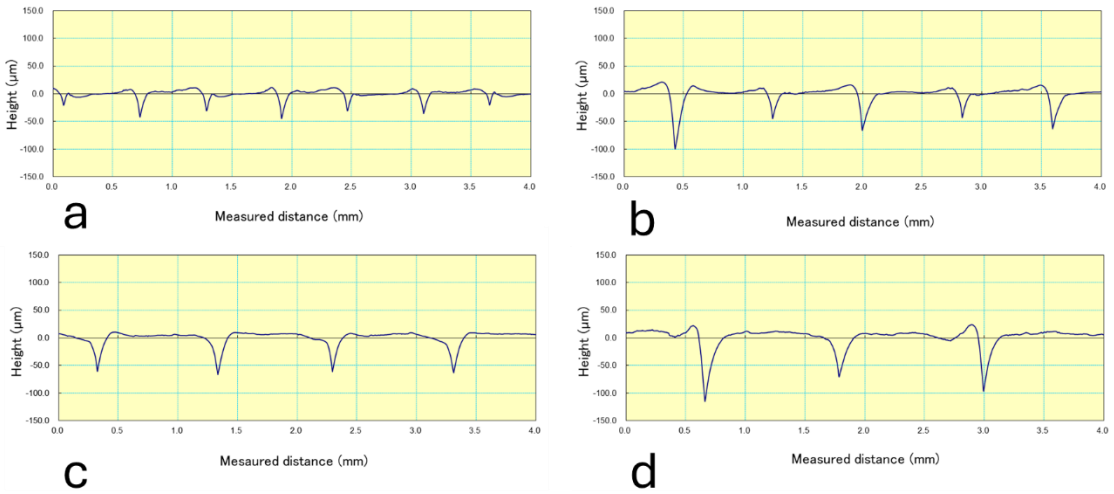

Figure 7. Surface profiles of 3D printed specimens with a line-width value of a) 0.6 mm, b) 0.8 mm, c) 1 mm and d) 1.2 mm.

Table 3. Measured surface roughness parameters of specimens

Line-width value (mm)	Ra (µm)	Rq (µm)	Rz (µm)
0.6	5.11±0.21	6.67±0.48	36.18±4.31
0.8	7.40±0.73	11.25±1.15	59.74±5.12
1.0	7.64±1.27	12.55±2.17	65.25±10.93
1.2	9.29±1.12	13.95±1.58	66.58±9.41

Stress-strain curves of 3D printed specimens by using different line-width values are shown in Figure 8. Tensile stress has a linear relationship with strain in the elastic zone. When the applied stress is removed, the material returns to its original shape within the stress-strain range shown by the linear zone. Beyond the linear-zone, the specimen undergoes plastic deformation and returning to original shape is not possible even after the applied stress has been removed. And at the end of plastic deformation zone, rapture of the specimen occurs [22]. The highest tensile strength value of 58.52±1.93 MPa with Young's modulus of 1.53±0.29 GPa was measured for the specimen printed with the line-width value of 0.6 mm. Tensile strength of the specimens printed with various line-width values decreased to 46.54±1.18 MPa with Young's modulus of 1.17±0.23 GPa for the specimen printed with line-width value of 1.2 mm.

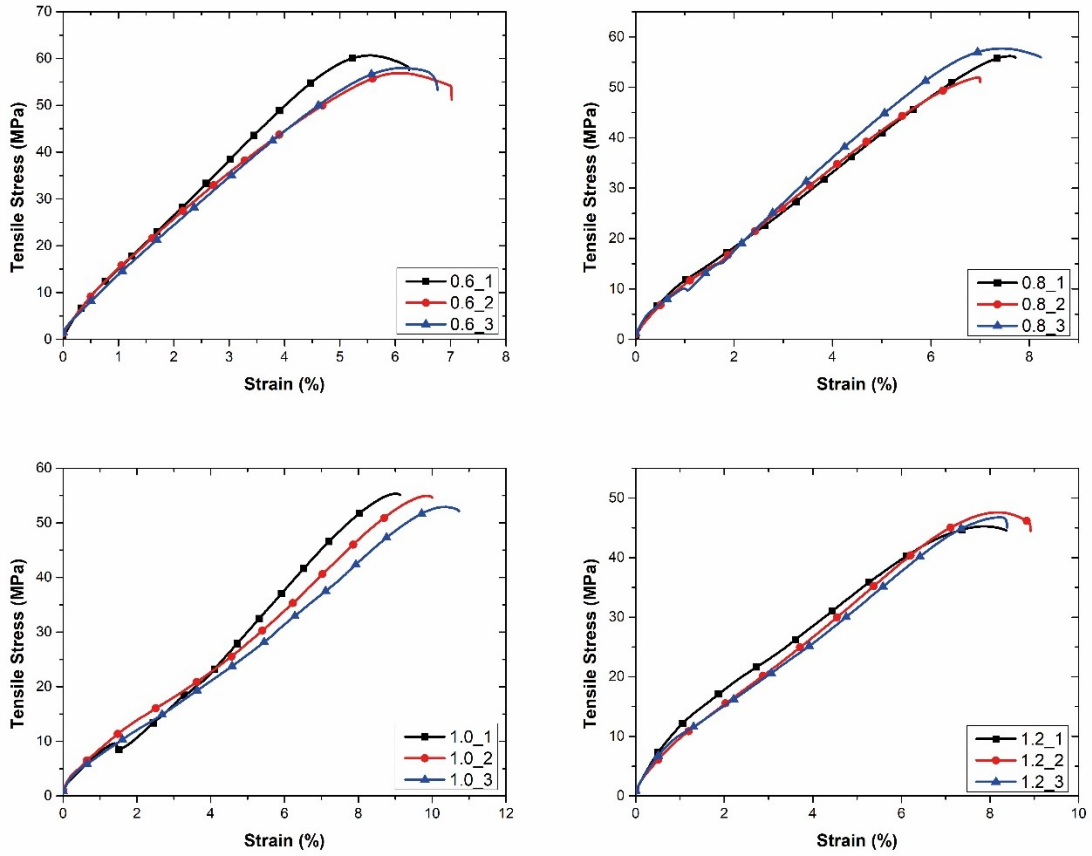

Figure 8. Stress-strain curves of 3D printed specimens by using different line-width values.

Shore-D hardness measurements results were given in Figure 9. Hardness value tended to decrease with increasing line-width value. Hardness value decreased from 44.16±4.21 to 35.80±2.95 for the parts printed using line-width values of 0.6 mm and 1 mm respectively. The hardness value increased to 41.66±3.51 for the specimen printed with line-width of 1.2 mm.

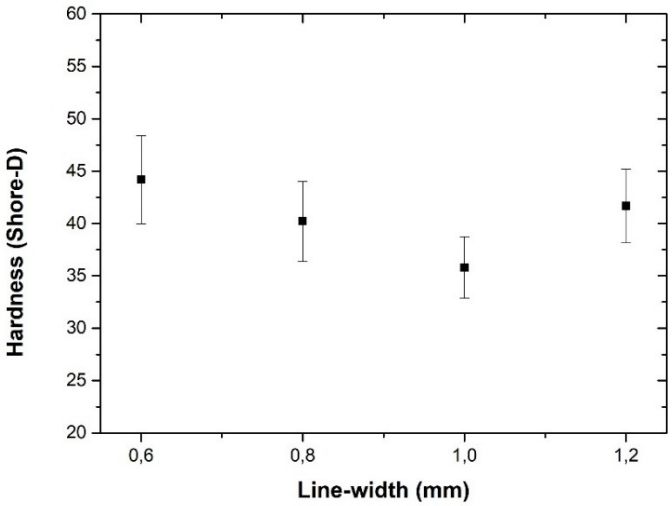

Figure 9. Effect of line-width value on the hardness.

The sliced images of specimens for line-width values of 0.6 mm and 1.2 mm are shown in Figure 10 a-d. It was observed that voids were formed between adjacent u-turns sections. The void between u-turns sections tended to become bigger when the line-width value increased from 0.6 mm to 1.2 mm. During tensile testing, these voids not only reduce the actual cross-sectional area under load but also behave as notches. Therefore, the slight diminish in tensile strength was attributed to the presence of voids between u-turn sections.

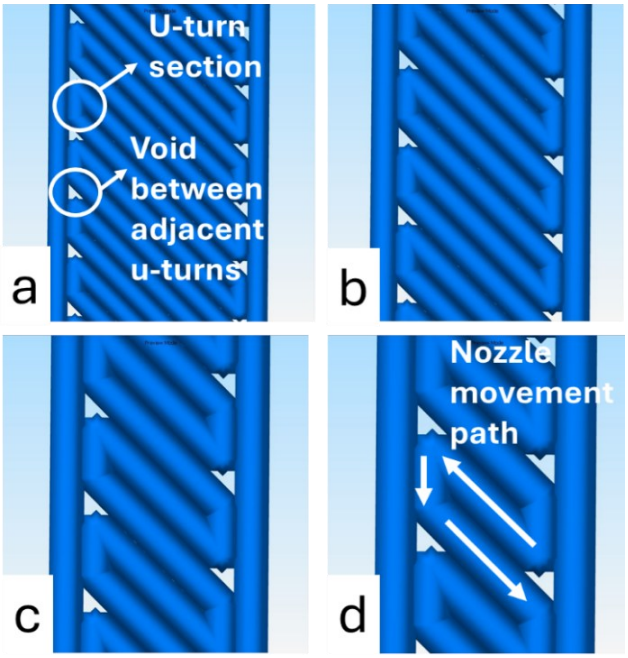

Figure 10. The sliced images of specimens for line-width values of a) 0.6 mm, b) 0.8 mm, c) 1 mm, and d) 1.2 mm

SEM images of tensile fracture surface of specimens printed with various line-width values are shown in Figure 11 a-d. SEM images of tensile fracture surface demonstrated that the main failure mechanism of the printed specimens was the rupture of deposited lines instead of fracture of inter-line bonding. It should be noted that u-turn section was clearly noticeable for the specimen printed with 1.2 mm line-width after tensile failure (see Figure 10 d).

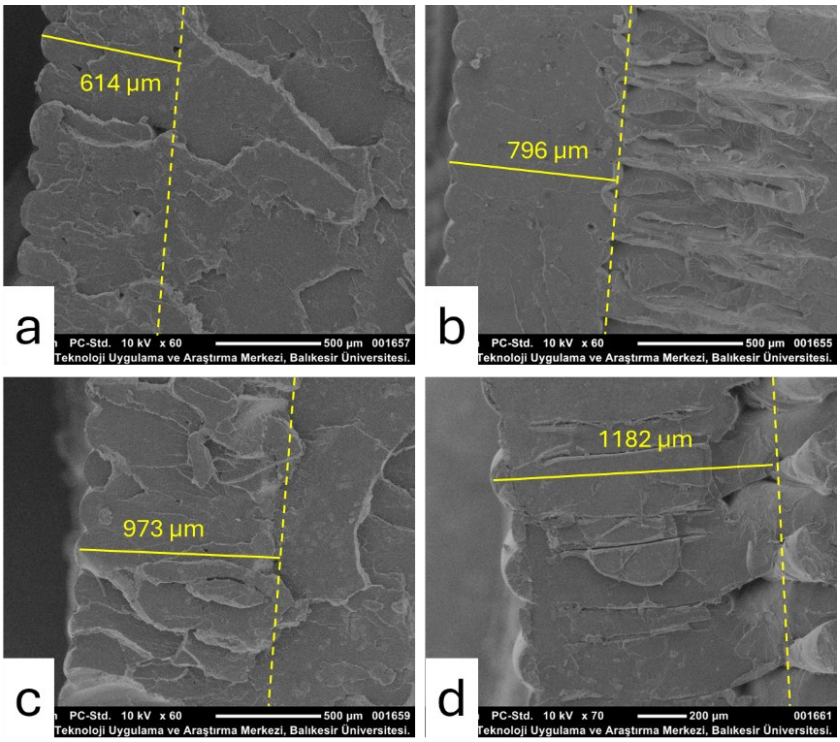

Figure 11. Tensile fracture surface of specimens printed with line-width values of a) 0.6 mm, b) 0.8 mm, c) 1.0 mm and d) 1.2 mm.

The calculated printing time for a cube with dimensions of 40 mm* 40 mm* 40 mm (x*y*z directions) with different line-width values are shown in Figure 12. As it is seen from the figure that the required time for the printing of cube decreased notably with increasing line-width. The 3D printing time for line-width of 0.6 mm was 226 min while the time for line-width of 1.2 mm was 114 min. The required printing time reduced nearly 49% with increasing line-width value from 0.6 mm to 1.2 mm. An area that would be printed with 2 pass with a line width of 0.6 mm can be printed in a single pass with a line-width of 1.2 mm. The printing time did not decrease exactly to 1/2 with the increase of line-width by 2 times. Since the time for the retraction of the filament and the time required for the nozzle to move to the printing start coordinates are also included in the printing time calculation. Therefore, printing time is not directly proportionate to line-width.

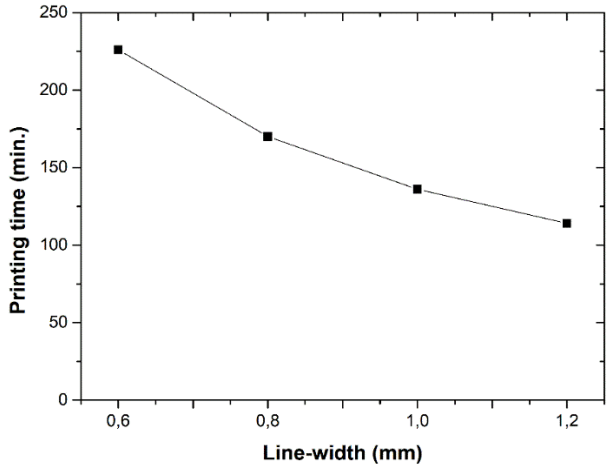

Figure 12. Line-width versus printing time curve (for the printing of 40*40*40mm cube)

4. Conclusion

In this study, the effect of line-width values on the properties of 3D printed PLA parts. 3D printing of parts such as tensile strength, surface profile and printing time. The following findings were observed:

- The void geometry did not change with increasing line width (except 1.2 mm), but the distance between the voids increased. It was observed that some lines were not deposited adjacent to each other and accordingly the void size increased in the Z axis, indicating poor bead to bead adhesion for line-width of 1.2 mm.
- Surface roughness parameter of Ra, Rq and Rz increased from 5.11±0.21 μm, 6.67±0.48 μm and 36.18±4.31 μm to 9.29±1.12 μm, 13.95±1.58 μm and 66.58±9.41 μm respectively with increasing line-width from 0.6 mm to 1.2 mm.
- The tensile strength and Young's modulus values decreased from 58.52±1.93 MPa and 1.53±0.29 GPa to 46.54±1.18 MPa and 11.17±0.23 GPa with increased line-width from 0.6 mm to 1.2 mm.
- Shore-D hardness value decreased from 44.16±4.21 to 35.80±2.95 for the parts printed using line-width values of 0.6 mm and 1 mm respectively. The hardness value increased to 41.66±3.51 for the specimen printed with line-width of 1.2 mm.
- The printing time required for the printing of a cube with a dimension of 40*40*40 mm reduced 49% with increasing line-width value from 0.6 mm to 1.2 mm.

References

[1] Türkoğlu, T., Functional grading of polymer triply periodic minimal surface structures for enhanced compressive performance and lightweight design in additive manufacturing. **Journal of Advances in Manufacturing Engineering**, 5(2), 94-102, (2024).

[2] Kim, D. B., Witherell, P., Lipman, R., & Feng, S. C., Streamlining the additive manufacturing digital spectrum: A systems approach. **Additive manufacturing**, 5, 20-30, (2015).

[3] Güler, S., Mechanical, Thermal, and Photocatalytic Properties of TiO_2/ZnO Hybrid Composites Fabricated via Additive Manufacturing. **Recep Tayyip Erdogan University Journal of Science and Engineering**, 5(2), 149-158, (2025).

[4] Jadhav, A., & Jadhav, V. S., A review on 3D printing: An additive manufacturing technology. **Materials Today: Proceedings**, 62, 2094-2099, (2022).

[5] Kantaros, A., Soulis, E., Petrescu, F. I. T., & Ganetsos, T., Advanced composite materials utilized in FDM/FFF 3D printing manufacturing processes: the case of filled filaments. **Materials**, 16(18), 6210, (2023).

[6] Osswald, T. A., Puentes, J., & Kattinger, J., Fused filament fabrication melting model. **Additive Manufacturing**, 22, 51-59, (2018).

[7] Arockiam, A. J., Subramanian, K., Padmanabhan, R. G., Selvaraj, R., Bagal, D. K., & Rajesh, S., A review on PLA with different fillers used as a filament in 3D printing. **Materials Today: Proceedings**, 50, 2057-2064, (2022).

[8] Chacón, J. M., Caminero, M. A., García-Plaza, E., & Núnez, P. J., Additive manufacturing of PLA structures using fused deposition modelling: Effect of process parameters on mechanical properties and their optimal selection. **Materials & Design**, 124, 143-157, (2017).

[9] Kuznetsov, V. E., Solonin, A. N., Urzhumtsev, O. D., Schilling, R., & Tavitov, A. G., Strength of PLA components fabricated with fused deposition technology using a desktop 3D printer as a function of geometrical parameters of the process. **Polymers**, 10(3), 313, (2018).

[10] Molina, A., & Acosta-Sullcahuamán, J., Effect of the Process Parameters on the Mechanical Properties of 3D-Printed Specimens Fabricated by Material Extrusion 3D Printing. **Engineering Proceedings**, 83(1), 1, (2025).

[11] Bhosale, V., Gaikwad, P., Dhere, S., Sutar, C., & Raykar, S. J., Analysis of process parameters of 3D printing for surface finish, printing time and tensile strength. **Materials Today: Proceedings**, 59, 841-846, (2022).

[12] Mulcahy, N., O'Sullivan, K. J., O'Sullivan, A., & O'Sullivan, L., Preliminary assessment on the effects of line width, layer height and orientation on strength and print time for FDM printing of total contact casts for the treatment of diabetic foot ulcers. **Annals of 3D Printed Medicine**, 11, 100115, (2023).

[13] Kim, M. K., Lee, I. H., & Kim, H. C., Effect of fabrication parameters on surface roughness of FDM parts. **International Journal of Precision Engineering and Manufacturing**, 19, 137-142, (2018).

[14] Butt, J., Bhaskar, R., & Mohaghegh, V., Analysing the effects of layer heights and line widths on FFF-printed thermoplastics. **The International Journal of Advanced Manufacturing Technology**, 121(11), 7383-7411, (2022).

[15] John, P., Komma, V. R., & Bhore, S. P., Development of MATLAB code for tool path data extraction from the G code of the fused filament fabrication (FFF) parts. **Engineering Research Express**, 5(2), 025018, (2023).

[16] Chen, J. M., Tseng, Y. Y., Lee, D., Lin, Y. T., Lin, S. H., Lee, T. Y., ... & Ito, H., A robust experimental model to explore the three-dimensional printing of polylactide parts: Solution versus melt extrusion. **Applied Sciences**, 10(2), 509, (2020).

[17] Suryanegara, L., Nakagaito, A. N., & Yano, H., The effect of crystallization of PLA on the thermal and mechanical properties of microfibrillated cellulose-reinforced PLA composites. **Composites Science and Technology**, 69(7-8), 1187-1192, (2009).

[18] Mysiukiewicz, O., & Barczewski, M., Crystallization of polylactide-based green composites filled with oil-rich waste fillers. **Journal of Polymer Research**, 27, 1-17, (2020).

[19] Shuhua, W., Qiaoli, X., Fen, L., Jinming, D., Husheng, J., & Bingshe, X., Preparation and properties of cellulose-based carbon microsphere/poly (lactic acid) composites. **Journal of Composite Materials**, 48(11), 1297-1302, (2014).

[20] Agustin, M. B., Nakatsubo, F., & Yano, H., The thermal stability of nanocellulose and its acetates with different degree of polymerization. **Cellulose**, 23, 451-464, (2016).

[21] Nasirov, A., Gupta, A., Hasanov, S., & Fidan, I., Three-scale asymptotic homogenization of short fiber reinforced additively manufactured polymer composites. **Composites Part B: Engineering**, 202, 108269, (2020).

[22] Alharbi, M., Kong, I., & Patel, V. I., Simulation of uniaxial stress–strain response of 3D-printed polylactic acid by nonlinear finite element analysis. **Applied Adhesion Science**, 8, 1-10, (2020).